Chapter 2

Instrumentation

All experimental setups used to test the dynamic behavior of granular systems are composed of three basic elements that are used to assemble, excite, and measure the response of the granular system of interest. Conventional experimental techniques employed for macroscopic granular systems include piezo transducers for applying excitation [16, 66], sensor particles embedded with accelerometer [9, 42, 63, 125, 126] for force measurements, and laser vibrometers [16, 127] for measurement of selected particles' displacement and velocity. Most of these methods cannot be directly applied or adapted to micro-granular systems. For example, force measurement based on sensors that are embedded in selected particles is not possible in micro-granular systems due to difficulties in fabricating micro-particles with embedded accelerometers. Also, piezo transducers cannot be easily used to drive micro-particles, because of the high-precision requirements related to controlling the nano-scale contact surface conditions and stiffness.

Assembling ordered granular systems is another challenge that emerges when the size of the systems is scaled down. Experimental studies of ordered granular materials require repeatable and regular means to assemble the particles in selected geometries/lattices. High accuracy in packing the particles is particularly necessary given the nonlinear nature of the contact interaction between each pair of particles. Increasing the number of particles in a lattice then creates increasing challenges in assembling a reproducible sample for testing. One-dimensional granular chains are easier to assemble, because the presence of a small pre-compressive force can compensate for small irregularities between particles. However, for two-dimensional systems, creating a "perfect" lattice is difficult even at the macro-scale [128], and disorder and misalignment between the particles can significantly alter wave propagation.

At the micro-scale, the precise control of the physical contact between particles is more difficult. The accuracy required to ensure repeatable tests increases rapidly as the particle size is reduced. At the same time, the physical contact between micro-particles is no longer exclusively governed by elastic interactions; particles exchange forces also through other potentials (such as Van der Waals), which

can be significantly altered by surface quality, geometry of the contact, and a variety of other factors that are difficult to monitor in real time. All of these issues that arise at the micro-scale call for the design of an ad-hoc experimental setup that reduces uncertainties that are related to the driving and measurement systems and that allows for a repeatable and controllable assembly of one- and two-dimensional samples. The rest of this chapter details the design of our new experimental system.

In our experimental setup (Fig. 2.1), we introduce non-contact excitation and measurement methods to avoid influencing the response of the system with intrusive driving and detection systems. We also design a computer-controlled robotic micro-manipulator to assemble the micro-particles automatically in selected lattice geometries, thus ensuring high-packing repeatability. The experimental setup designed for this thesis consists of three major components: (i) The sample holders and the micro-manipulator system, which confine and assemble the micro-particles in precise locations; (ii) the excitation system, which delivers controlled momentum to a target particle using a Q-switched, nanosecond pulsed laser that is operating in single-shot mode; and (iii) the measurement system, which consists of laser vibrometry and high-speed microphotography. In this chapter, we discuss the sample preparation and the measurement systems. The excitation of the micro-particles is discussed in more detail in the next chapter.

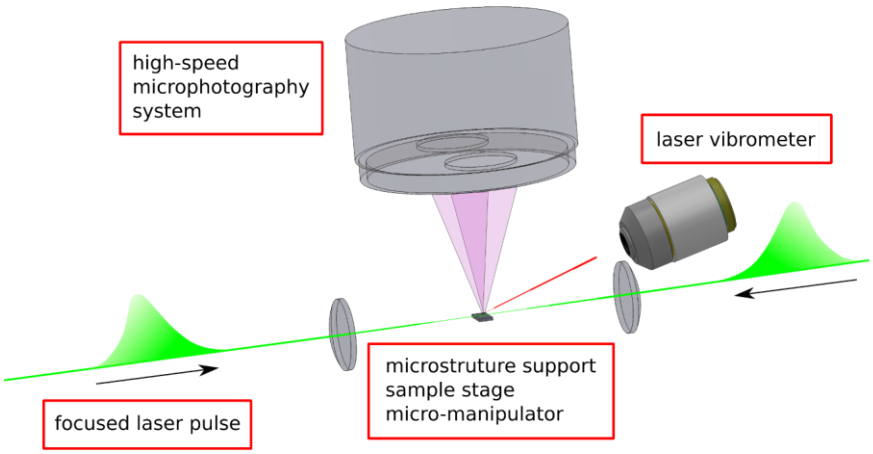

Figure 2.1: Overview of the experiment scheme. The apparatus consists of three major parts, including the excitation system (focused laser pulse), the measurement system (high-speed microphotography and laser vibrometry), and the sample assembly and manipulating system.

2.1. Particle confinement and sample stage

In this thesis, we focus on micro-particle systems that are assembled in one- and two-dimensional configurations. Two specific types of systems are investigated: (1) dry, one-dimensional granular chains that consist of stainless steel particles with a radius of 150μm, and (2) wet, two-dimensional systems that consist of silica spheres with a radius of 3.69 μm that are immersed in a water-glycerol solution with variable viscosity. For testing these two systems in the selected configurations, it is necessary to design specific supporting structures that guide and confine the movement of micro-particles. For the experiments on dry particles, we fabricate appropriate v-shaped supports using photolithography on a silicon wafer. To assemble two-dimensional, close-packed arrays of colloids in fluids, we use commercially available micro-fluidic cells as supports.

Once the micro-particles are loaded on the desired support structures, the experimental apparatus needs to (i) record the initial particle-configuration by identifying and locating all of the particles and (ii) modify the initial configuration to the particle-configuration of interest, which entails moving, positioning, and pre-compressing the micro-particles to ensure physical contact between them. As described in detail later, we perform this operation using a microscopic imaging system and a micro-manipulator.

We then mount the samples on a computer-controlled sample stage that consists of a pitch and roll platform (Thorlabs APR001) that is installed on a three-dimensional motorized stage (zaber T-LSM025A). The sample stage is leveled with an inclinometer (Level Developments IS-2-30) with an accuracy of 0.1°, which allows us to induce particle movement by tilting the stage. This sample stage reduces the difficulty of handling and manipulating the systems of micro-particles. In the following subsections, we explain the experimental construction of the two micro-granular systems (i.e., the dry and wet micro-granular systems) that are analyzed in this work.

2.1.1. One-dimensional micro-granular systems

The one-dimensional micro-granular systems considered in this thesis consist of micro-particles that are made of two different stainless steel materials, namely grade 316 and grade 440c. We list the dimensions and properties of these materials in Table 2.1. The two particles being studied both have a 300 μm diameter; their other similar physical properties include density, elastic modulus, and Poisson ratio. The most significant difference between them is surface roughness, which is an important source of imperfections in micro-granular chains. According to the specifications provided

by their manufacturers, the stainless steel 316 particles have a nominal surface roughness of 3 μm, while the 440c particles have a smaller surface roughness of 0.1 μm. The difference in surface quality can be seen in the scanning electron microscope (SEM) images of the two particles in Fig. 2.2. As we show in the following chapters, systems made of the higher surface quality particles of stainless steel 440c have a mechanical response that better agrees with the theoretical and numerical predictions of granular systems that are composed of ideal particles. Another noticeable difference between the two types of particles is their thermal conductivity; stainless steel 440c has a nominal thermal conductivity (24.2 W/mK) that is about 50% higher than that of stainless steel 316 (16.3 W/mK) [129]. This affects the efficiency of the laser excitation we used to drive the system, which is discussed in Chapter 3.

Due to the small size and mass of the individual micro-particles, configurations of micro-granular systems are vulnerable to static charges and external magnetic fields. Electrically charged particles strongly repel each other and cannot be arranged in an ordered lattice. To avoid these issues, all particles are rested on a conducting metal disk to remove unwanted static charges before they are assembled into specific configurations. Magnetic fields, even those generated by magnetic objects such as metal tools, attract the stainless steel 440c particles. To avoid magnetic interferences during assembly, we transport the particles to the supporting structures with either a very light blow of compressed air or tweezers made of non-magnetic materials.

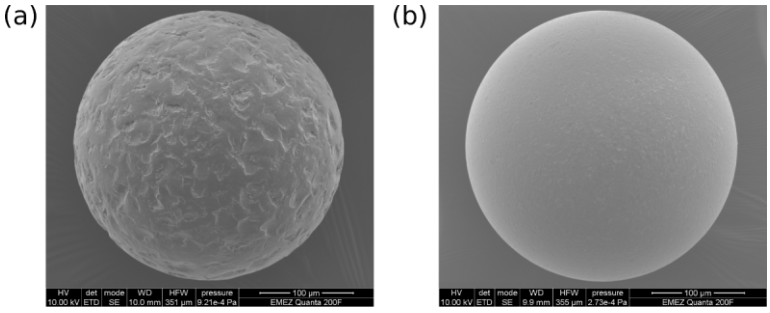

Figure 2.2: An SEM image of micro-particles used in this experiment. (a) Stainless steel 316 particle with a radius of 150 μm and surface roughness of 3 μm. (b) Stainless steel 440c particle with a radius of 150 μm and surface roughness of 0.1 μm.

Material properties	Stainless steel 316 particle	Stainless steel 440c particle
Radius (μm)	150	150
Radius variation (±μm)	2	1
Surface roughness (μm)	3	0.1
Density (kg/m^3)	7990	7650

Elastic modulus (GPA)	193	200
Melting point (K)	1660	1760
Thermal conductivity at 100C (W/mK)	16.3	24.2
Specific heat (J/kg/K)	510	460

Table 2.1: Dimensions and material properties of our stainless steel micro-particles [129, 130]. Particles made of stainless steel 316 and 440c are used in this work. These two particles have similar physical properties except for the significant differences in surface roughness and thermal conductivity.

To create a one-dimensional micro-granular system, we deposit the particles on v-shaped grooves that are fabricated on silicon wafers. The grooves constrain the particles from moving along the axis of the groove. The fabrication procedures are shown in Fig. 2.3a. Starting with a [100] silicon wafer with a thickness of 1 mm, we deposit a 1 μm thick layer of silicon nitride (Si_3N_4) on the surface via chemical vapor deposition. The wafer is then patterned with 1.6 μm of AZ5214 positive photo-resist, before the silicon nitride layer is opened up with reactive-ion etching (RIE) techniques. The wafer is subsequently treated with a 50% potassium hydroxide (KOH) solution at 85ºC to perform anisotropic chemical etching. This etching process removes unmasked silicon, reveals the [111] crystal planes, and forms v-shaped grooves (Fig. 2.3b). The grooves we use in the experiments have a width of 240 μm and we estimate the surface roughness to be 0.1 μm according to the fabrication process [131]. The angle between two inclined [111] planes is 70.6º.

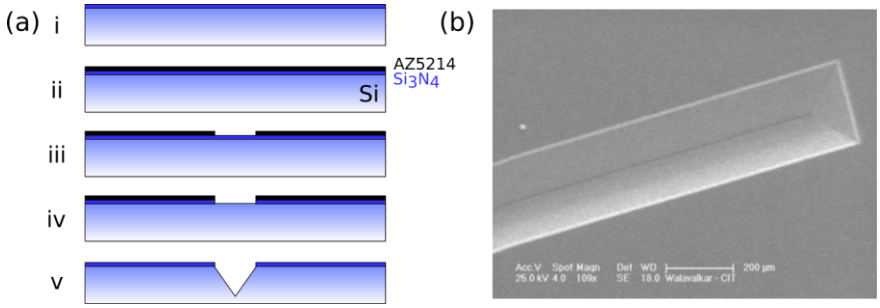

Figure 2.3: Micro-fabrication process of one-dimensional v-shaped grooves with a width of 240 μm and an inclined angle of 70.6º. (a) Overview of the fabrication process: i) Chemical vapor deposition of a 1μm thick layer of silicon nitride (Si3N4) on the surface of a 1mm thick silicon wafer [100]. ii) Spin coating with 1.6 μm of AZ5214 positive photo-resist. iii) Exposing and developing the photo-resist. iv) Patterning the silicon nitride layer with reactive-ion etching (RIE). v) Anisotropic chemical etching with a 50% potassium hydroxide (KOH) solution at 85ºC. (b) An SEM image of the resultant v-shaped grooves.

Once the particles are placed in the v-shaped groove, we manipulate them with a computer-controlled micro-manipulator to align them and secure contact between them. The micro-manipulator consists of a sharp tip (a stainless steel micro-wire with a tip size of 100 μm) that is installed on a three-dimensional motorized stage (zaber T-LSM025A). The micro-manipulator moves the micro-particles by physically pushing them from one side. The position of the micro-particles is determined by image processing, using a microscopic photography system. The sequences of the micro-manipulator movements are determined by a control program. The motion is determined based on the difference between the current configuration (as detected by the imaging system) and the desired configuration (which is preset in each experimental run). More details concerning the particle manipulation procedures are given in Section 2.5.

To construct a micro-granular chain, we use our computer-controlled sample stage and the micro-manipulator system to assemble close-packed micro-particles in a v-shaped groove. We start by loading the particles randomly into the v-shaped groove, after which we blow along the groove with compressed air to form a loose chain of particles. To minimize the gap between particles and create a close-packed chain of micro-particles, we tilt the computer-controlled sample holder by 10° from horizontal place while simultaneously positioning the micro-manipulator to the lower end of the groove to block the free-moving particles from rolling out (see Fig. 2.4). After particles form a close-packed granular chain, we slowly tilt the sample stage back to a horizontal position and withdraw the micro-manipulator carefully so as not to disturb the chain.

To characterize the assembled chain before each measurement, we acquire microscopic digital images to record the initial position of each particle. Using photographs taken by our imaging system (Fig. 2.4b), we determine the location of the particles at a 2 μm accuracy with an image-processing algorithm similar to what was mentioned in Chapter 2. Since gaps between particles can be as small as tens of nanometers, which is far below the diffraction limit of our imaging system, the image-processing algorithm cannot resolve the presence of individual gaps. However, by measuring the total length of the micro-particle chain, we can estimate an upper bound of the average gaps that are present within the chain. According to the specifications provided by the manufacturer [130], the stainless steel 440c micro-particles used in our experiments have a variation in radius of $\pm$1 micrometer. In a chain that is composed of 15 particles, the resulting uncertainty in the total length of the chain is $\sigma_{total\ length} = 2\sqrt{15-1}\sigma_{radius}$ micrometer. After the construction of micro-chains, if we opt to

test only the chains that have a total measured length that is below average, we can estimate that the upper bound of the average gap is not larger than $2\sqrt{14}\sigma_{radius}/14 = 500\ nm$.

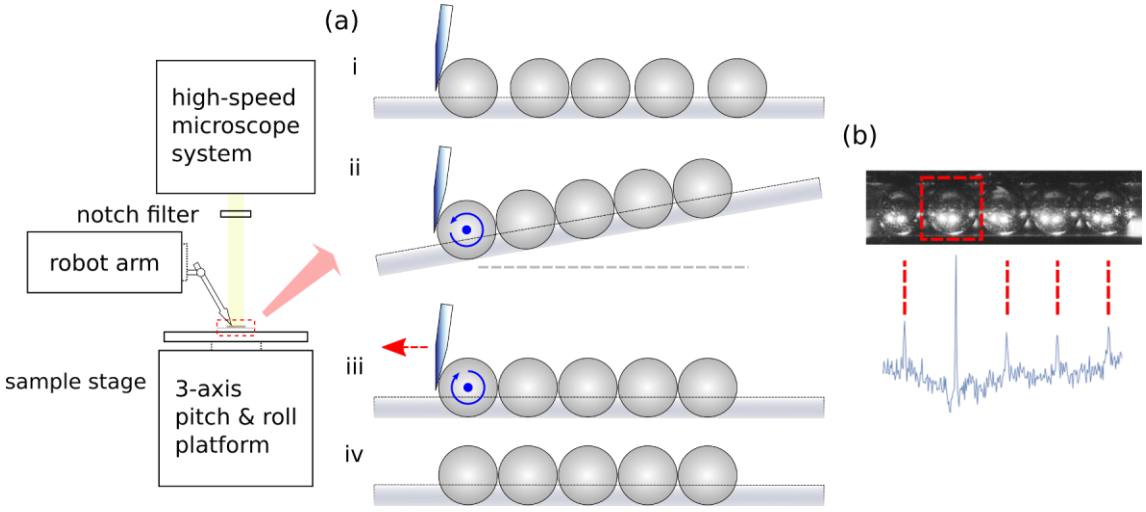

Figure 2.4: Procedures for assembling a micro-granular chain. (a) i) Micro-particles are positioned loosely in a v-shaped groove. ii) The sample stage is tilted to create a close-packed granular chain, blocked at one end by a robotic tip. iii) The sample stage is tilted back horizontally and the tip is withdrawn. (b) Optical imaging system to determine the locations of the particles using an image-processing algorithm. The image of the particle in the red box is used as the kernel of the image deconvolution, to reveal the position of other particles. The blue curves below show the results of the deconvolution algorithm, through which the other four particles are detected. A particle's position can be obtained with 2μm accuracy.

2.1.2. Two-dimensional micro-colloidal systems

Another type of micro-granular system that we investigated in this thesis is the two-dimensional system of colloidal particles immersed in fluid. The micro-particles (MicroParticles GmbH) are SiO_2 particles with two different radiuses (Table 2.2) of 3.69 and 3.14 μm. These two types of particles differ slightly in size and mass but have the same material properties.

Material properties	SiO_2 particles 1	SiO_2 particles 2
Radius (μm)	3.69	3.14
Radius variation (μm)	0.12	0.12
Refractive index	1.42	1.42
Density (kg/m3)	1850	1850
Elastic modulus (GPA)	73	73

Table 2.2: Dimensions and material properties of the colloidal particles used in the wet, two-dimensional experiments.

The supporting structures used to confine the two-dimensional motion of the SiO_2 particles is a commercially available micro-fluid cell (Hellma Analytics, Fig. 2.5a) that has a high quality quartz interior flat surface. Two-dimensional ordered granular systems are created within the cell using self-assembling techniques: after the particles are first injected into the cell with water, we tilt the cell to 5° along the long axis of the horizontal plane (Fig. 2.5b). After the particles cumulate on one side (Fig. 2.5c), the cell is tilted back to a horizontal position, which allows the piled up particles to relax and slowly move back toward the other side of the cell. In this relaxation process, micro-particles can form a hexagonal lattice after the system is stabilized. In Fig. 2.5d, we show the hexagonal lattice that is created. The dark particle in the center is a particle that is coated with a metal layer to enhance its interaction with the laser excitation system, which we explain in Chapter 3.

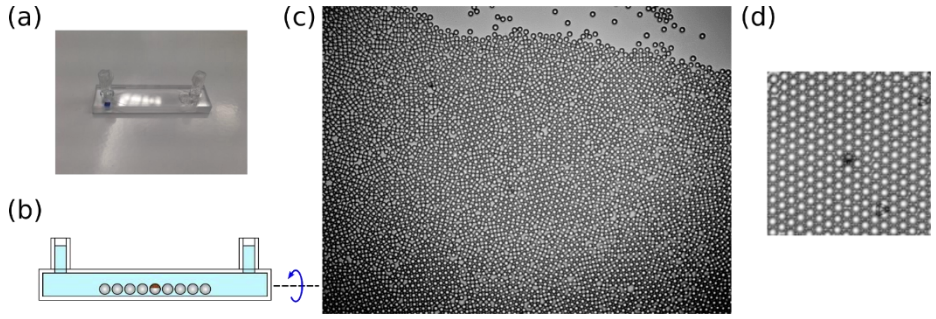

Figure 2.5: Preparation of two-dimensional micro-colloidal systems of SiO_2 particles. Hexagonal lattices are created by self-assembling techniques. (a) The micro-fluid cell used in this experiment. (b) A schematic diagram of the cell tilting process. (c) A digital image of dense, disordered micro-particles in the cell at the beginning of the relaxation process. (d) The final hexagonal lattice with a coated particle in the center.

2.2. Laser power controlling and beam conditioning

The mechanical excitation of the micro-particles is obtained with a focused, high-power laser beam that targets the surface of selected particles. The temperature rise that is induced by the focused pulsed energy results in the vaporization and removal of the particles' surface materials. This phenomenon is known as pulsed laser ablation (PLA). When ablation is induced on the surface of a micro-particle, the reaction force from the ablated material pushes the particle forward. The momentum transferred to the targeted particles is proportional to the velocity of the ablated materials, as well as to the mass

of the vaporized surface materials. With this technique, we can deliver controlled impulses to selected particles that result in the motion of these particles with a controlled initial velocity. We look into the details of the ablation process in Chapter 3; here we just focus on the optical systems that guide the laser beam to the sample.

The laser system is responsible for producing accurate, repeatable mechanical excitations to the system of micro-particles. The requirements for performing reproducible experiments are proper conditioning of the beam profile, control of the laser power, and focusing. The laser system in use is a 532 nm wavelength, Q-switched Nd:YAG nanosecond laser (Quantel Brilliant) with a maximum power of 3.2 W. The laser beam has a linear polarization and energy stability of 2% and the pulse duration is 4 ns. To improve beam quality and focusability, we install a spatial filter (Thorlabs KT310) at the output of the laser beam to create a clean Gaussian beam profile.

The total laser beam output can be controlled manually by an internal attenuator that is located inside the laser body. Since the maximum laser power achievable by our system is too high for the optimal range of operation of our experiments, to prevent excessive damage to the sample we limit the actual output of the laser to 5 mW. The beam is then passed through a combination of a half-wave plate and a polarized beam splitter to further control the laser power that will be delivered to excite the sample. The beam is split into two by a polarized beam splitter. In one arm the beam is sent to the sample holder, while in the other arm it is monitored by a power meter. The ratio of the power of the input beam, I, to the power of the output beam, I_1, is determined by the angle between the axis of the half-wave plate. The polarized angle of the beam, θ. I_1 can be expressed as: $I_1 = I(\frac{1}{1+v} + \frac{v}{1+v}\sin(4\theta - 4\theta_0))$. Here v is visibility and θ_0 is a constant offset that depends on the polarization angle of the laser beam and on the angle of the polarized beam splitter.

Before experiments are conducted, the laser power is calibrated at different θ to retrieve accurate values of v, I, and θ_0. This process allows us to accurately control the output power. The control of the laser power is also enhanced by the computer-controlled motorized rotational stage (Thorlabs PRM1Z8, PRM1Z8E) that supports the half-wave plate. The motorized stage has an angular resolution of 0.03º, which corresponds to a power resolution of 0.1% of the maximum power. A computer-controlled optical shutter (Thorlabs SH05, SC10) is also installed to block and prevent the beam from damaging the samples when the laser is operating.

2.3. Measurement system

The dynamic response of the micro-particles on the sample stage is measured by two independent methods: a laser vibrometer and a high-speed microscopic imaging system. We use a laser vibrometer to measure the velocity of the micro-particles and use the high-speed imaging system to measure the trajectory of the micro-particles.

2.3.1. Laser vibrometry

Laser vibrometers measure the velocity of the targeted surface via Doppler effects of reflected laser beam from the target. Considering the surface curvature of our micro-particles, it is necessary to focus the beam to a size much smaller than the particle's radius. For focusing the laser beam to a 3μm spot size, we install an objective lens (Mitutoyo PLAN APO 10x) on the vibrometer.

The laser vibrometer (Polytec OFV-534, OFV-5000) can achieve a resolution of < 1 pm and has a maximum sampling frequency of 2.5 MHz in DC mode and 24 MHz in AC mode. The output of the vibrometer is recorded by a high-speed data acquisition system (AlazarTech ATS9462) at a maximum acquisition rate of 180 MS/s, which is higher than the upper limit of the frequency band of the vibrometer.

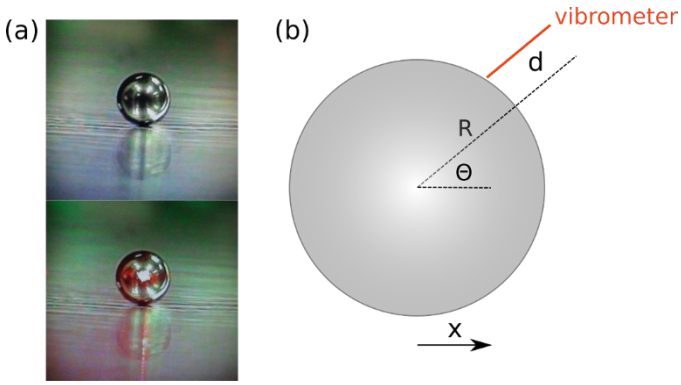

Figure 2.6: (a) Photograph of a laser vibrometer shining on the surface of particles with a radius of 150μm; the beam waist of the vibrometer beam is 3μm. (b) Schematic diagram of a realistic use case of a vibrometer being used on micro-particles. The red line indicates the beam of vibrometer, while d is the offset of the beam to the center of the particle and θ is the angle between the particle displacement, x, and the laser beam.

The requirements of laser focus on the particles impose many restrictions on the experiments that can be conducted. The vibrometer can only be focused on particles that are lying within the laser's focal

plane. This limits the ability to use the vibrometer to track moving particles, as these particles move rapidly out of the field of view. As a result, the range of displacement acquisitions is limited to only the first few μm of the micro-particle's motion.

The size and surface curvature of the micro-particles also introduce additional complexity to the measurements (Fig. 2.6b). Because of the limitations dictated by the physical geometry of the experimental system, the laser vibrometer is usually pointed at the particles with an inclined angle that is between 10º and 40º with the horizontal place. Since Doppler effects only account for the motion of the particle parallel to the axis of the vibrometer's beam, we expect the measured velocity to be different from the real particle velocity (which is along the horizontal plane).

This problem can be accounted for by measuring experimentally the ratio between the measured velocity and the actual velocity. In our measurements, we obtain a correction factor by measuring the displacement of the particle on the sample stage while moving the stage by computer in a known direction and distance (Fig. 2.7). The ratio between the two can be used to correct the velocity data obtained by the vibrometer. Typically, the correction factor for a given system configuration is calculated between 0.6 and 0.9; it is mostly affected by the inclined angle of the vibrometer. Using the symbols defined in Fig. 2.6b, it is not difficult to derive the following formula for the displacement $d^{(m)}(d)$ as measured by the vibrometer:

$$d^{(m)}(d) = \sin(\theta)^2\sqrt{1+\tan(\theta)^2}\,(x\cot(\theta)^2 - \sqrt{(-d^2+R^2)\,\cot(\theta)^2\,\csc(\theta)^2} + \sqrt{\cot(\theta)^2\left(R^2\cot(\theta)^2 + \big(R-x-d\,\csc(\theta)\big)\big(R+x+d\,\csc(\theta)\big)\right)}), \quad (2.1)$$

where x is the displacement of the particles, θ is the angle between the beam direction and the particle displacement, d is the offset of the laser beams to the particle center, and R is the particle radius. This formula also indicates that the measured velocity is linearly proportional to the actual particle velocity and that the inclined angle dominates the correcting factor.

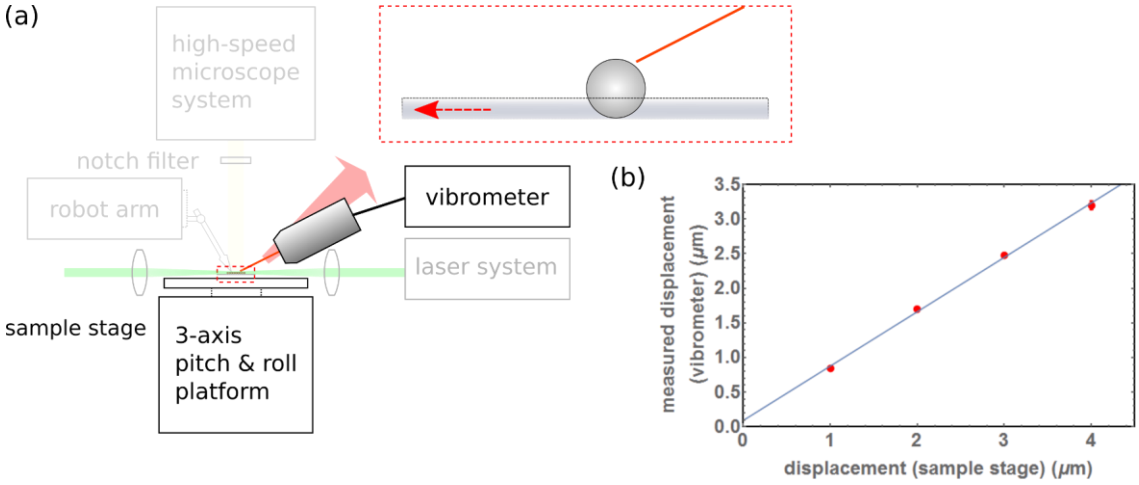

Figure 2.7: Calibration of vibrometer output. (a) Calibrations are performed by focusing a laser beam on the surface of a micro-particle and then using the computer-controlled sample stage to move it along its expected direction of motion in experiments (i.e., along the axis of the v-shaped groove). (a) The measured displacement (red dots) compared with the displacement of the sample stage (and the particle). The slope of the (blue) fitting line shows that there is a factor of 1.24 between the output velocities of the vibrometer and the real velocities in the horizontal plane.

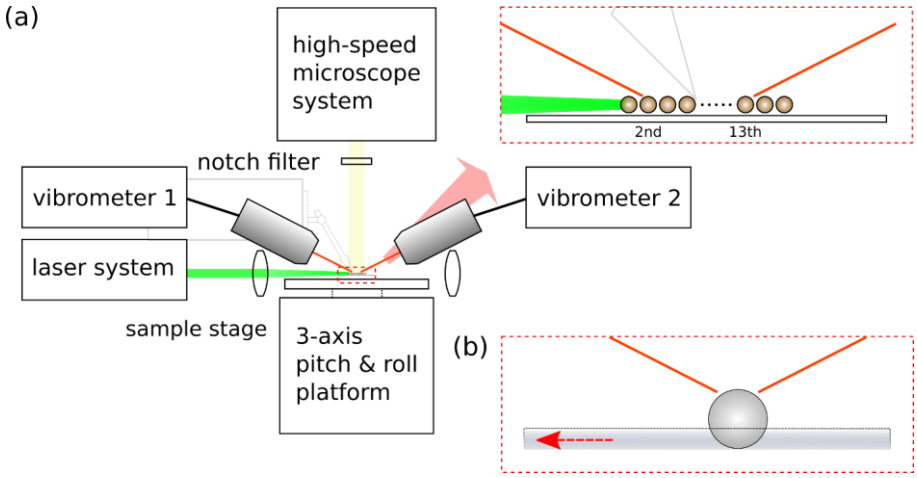

Figure 2.8: Schematic diagram of the experimental setup. (a) Two laser vibrometers are pointed on the micro-granular chain that is constructed with the procedures shown in Fig. 2.4. The granular chain consists of 15 particles and the vibrometers are pointed at the 2nd and 13th particles. (b) Calibration of vibrometer output. Two vibrometers are focused on the same particle. To calibrate vibrometer measurements, we point two vibrometers on the same particles and measure the relative time delay in output signals.

In Chapter 5, we measure the wave speed of the pulses traveling through the chain. Two vibrometers are used to measure the motions of two separate particles in the chain, and we measure the difference in arrival time (Δt) of the traveling wave at these two locations, as shown in Fig. 2.8. Due to the constraints on the available workspace, the two vibrometers need to point at the particles in the chain at different angles and in opposite directions along the groove (Fig. 2.8a). Besides the different output amplitudes caused by the different angles of the laser beams, processing the signal introduces an additional time delay of a few microseconds to the output signals of each vibrometer. In order to ensure meaningful comparison of the output signals of the two vibrometers, calibration must be used to determine both the time delay between the two output signals on the same event and the output voltage level for both vibrometers of the same particle velocities along the axis of the chain. The calibration process is similar to what we describe in the case of one vibrometer, except in this case two vibrometers need to be calibrated using the same object (Fig. 2.8b). To do this, the two vibrometers are moved to focus on the same particle (while maintaining the same angle to the chain); and the target particle is then moved with the computer-controlled sample stage. From reading the voltage output of both vibrometers, we know the scaling of the output signals, as well as the time delay between the outputs of the two vibrometers

2.3.2. High-speed micro-photography

We use high-speed cameras (Vision Research Phatom v12.1 and v1622) to record the trajectories of micro-particles that are excited by a controlled impact. After acquisition, the images are analyzed with an image-processing program to extract the displacement and velocity of the particles in the system. In this work, we deal with two micro-granular systems at two very different length scales (stainless steel particles of radius 150 μm and SiO_2 particles of radius 3.69 μm); different optical lens systems are therefore used for the best results in both cases.

Imaging the dry micro-particles requires a large field of view in order to capture sharp images of all of the stainless steel micro-particles that contribute to the dynamics. To accomplish this, the high-speed camera is equipped with a microscope (Leica S6D) with a large depth of field and achromatic lens pairs (Thorlabs MAP1050100-A) and is aligned and mounted vertically on top of the sample stage. A notch filter with a 532 nm central wavelength is installed to protect the CMOS sensor of the camera from the focused laser beam. The imaging system provides a spatial resolution of 4.3 μm per pixel and the field of view is 5.5 x 3.4 mm^2. The acquisition rate is limited by the shortest feasible

exposure time (39 µs in our system), which depends on the available illumination (we use a Fiber Optic Illuminator, 250 W). In our setup we achieve a maximum acquisition rate of 25,000 fps.

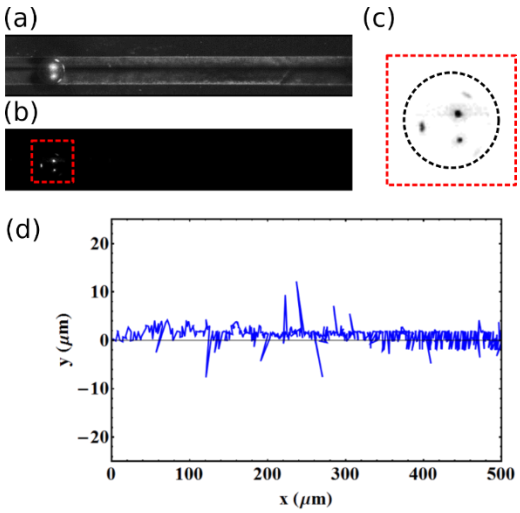

Figure 2.9: Image processing of the high-speed image sequence of a micro-particle moving on a groove. (a) Image of a micro-particle in a microstructure with an exposure time of 990 µs. (b) Image of the same particle with an exposure time of 39µs. (c) A portion of (b) is manually selected for use as the kernel of the deconvolution algorithm. (d) Resultant trajectory of the micro-particle moving under the camera.

To extract quantitative information from the high-speed images, we write an image-processing program to automatically detect a particle's position and measure its velocity. Each frame in the high-speed image sequence is deconvoluted to identify relevant tracking features and record the particle's position. Figure 2.3a shows typical high-speed images obtained when a single particle positioned in the v-shaped groove is moving. In this acquisition, the high-speed camera was operated at 1,000 fps with an exposure time of 990 µs. By decreasing the exposure time to 39 µs (25,000 fps), a higher time resolution can be obtained (Fig. 2.9ab). In this case the illumination is not sufficient to provide a clear view of the particle's edges and the particle's position is tracked following reflected light spots on the particle's surface. The image of the particles that is shown in the red box of Fig. 2.9b,is selected manually and used as a reference point for the particles in low light conditions.

Starting from the first frame, our program searches the next frame in the movie for areas that are similar to the image of the particles in the previous frame. We use image deconvolution to resolve the location of such areas and therefore the location of the particles. The particles' positions are then updated at each time step by searching for the trackers within a small window of their previous

position. Typical particle tracking results are shown in Fig. 2.9d. Because the deconvolution algorithm utilizes 50 x 50 pixels of information for each particle, the location of the particles can be determined with a sub-pixel accuracy. The observation can be confirmed in Fig. 2.9d, where the fluctuation of particle location is about 2 μm (which is less than the image resolution of 4.2 μm). A particle's velocity can be calculated by dividing its travel distance by the exposure time.

For the wet particles, we use a commercial available lens tube (Infinity) with a microscope lens (NIKON LU Plan Fluor EPI P 20x) to achieve micro-scale image resolution. We obtain a spatial resolution of 0.90 μm per pixel and a depth of field of a few μm. With the illuminating light now focusing on a much smaller area, we are able to acquire clear images at an exposure time of 2.7 μs and a maximum of 311111 frames per second, with a resolution of 128 x 128 during typical data acquisitions.

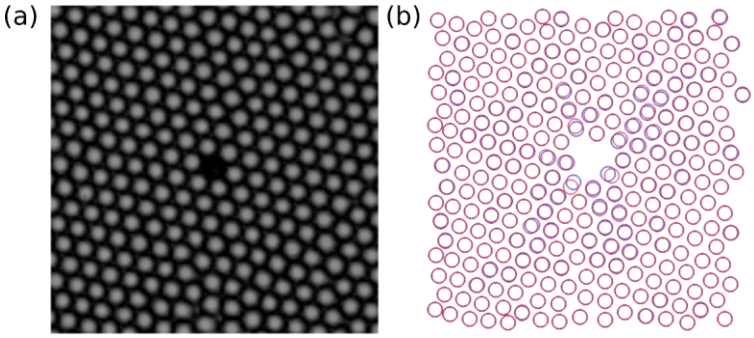

Figure 2.10: A typical high-speed image of the wet two-dimensional micro-granular system and the results of image processing. (a) Image of a micro-particle in a microstructure with an exposure time of 2.7 μs. (b) Resolved positions of colloids with image processing algorithm. The blue circles are the initial positions at t=0, while the red circles are the positions after 3.3 μs.

The particles are tracked with an image processing software following a working principle that is similar to the one used in the case of dry particles. In Fig. 2.10, we show the images obtained by the high-speed imaging system (Fig. 2.10a) and the resolved particle positions in the frame before (blue circles) and after (red circles) the system is excited by the laser. Notice that the resolved particle positions (Fig. 2.10b) do not contain all of the particles in the original photography (Fig. 2.10a). This can occur when some particles move out of the focal plane of the camera, or when some particles move too fast for the program to capture.

2.4. Configuration of the laser focusing system

The high-power laser beam is used to deliver controlled momentum to the micro-particles in different configurations. Since the samples tested vary significantly in their requirements and geometric assemblies, the laser beam configuration is also different in each case. The following subsections provide more details of each sample's design and utilization.

2.4.1. One-dimensional micro-granular systems

In Fig. 2.11, we plot the laser configuration used to excite the dry micro-particle chains. Before the laser beam reaches the micro-particles, it is focused with a lens that has a 60 mm focal length and a beam waist of 15 μm at the focal point. In order to ensure that the particles gain their momentum along the groove, the beam needs to be aligned to shine into the v-shaped groove in order to reach the outer-most particle.

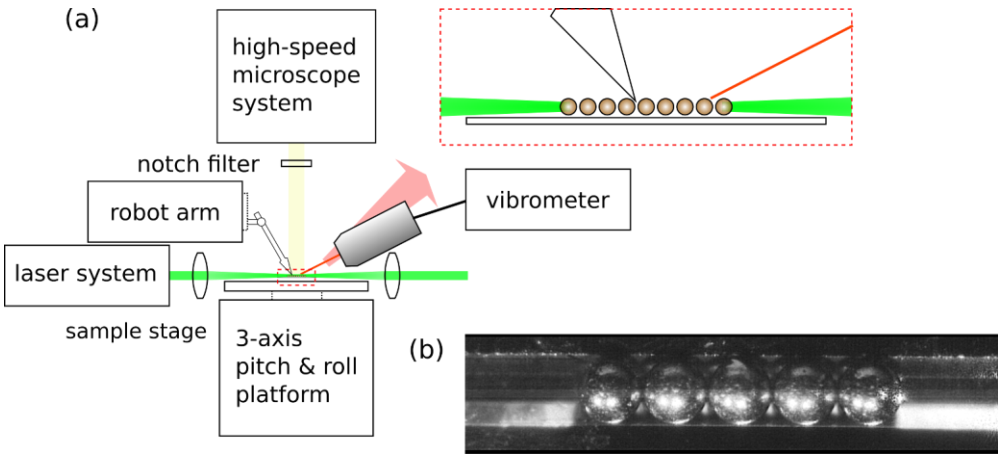

Figure 2.11: Experiment configuration for one-dimension micro-granular systems. (a) Micro-particles loaded on the supporting structure are assembled to the desired configuration by the computer-controlled micro-manipulator. The samples are monitored with a high-speed imaging system above the sample holder and a vibrometer that is pointed at the surface of a micro-particle. The focused laser beam with 15 μm is aligned to shine at the outer-most surface of the particle to excite the sample. (b) One-dimension micro-granular chain assembled in a v-shaped groove.

2.4.2. Two-dimensional colloidal hexagonal lattices

In Fig. 2.12, we show the laser configuration we used to excite the wet micro-particle systems. The SiO_2 micro-particles are arranged in hexagonal lattices in a micro-fluidic cell made of transparent material (quartz). The transparent material used for the cell allows the laser beam to transmit through

the cell from below. The laser beam is merged with the illumination and passes through an objective lens (Mitutoyo 20X) to focus at the same focal plane of the high-speed imaging system (which is also the location of the micro-particles). The laser is targeted at the dark particle in the center of Fig. 2.12b, which is an SiO_2 particle coated with a metal layer (non-transparent). The resulting dynamic response is monitored by the high-speed imaging system above the sample stage, which is protected by a notch filter that is blocking the pulsed laser from the sensor of the high-speed camera.

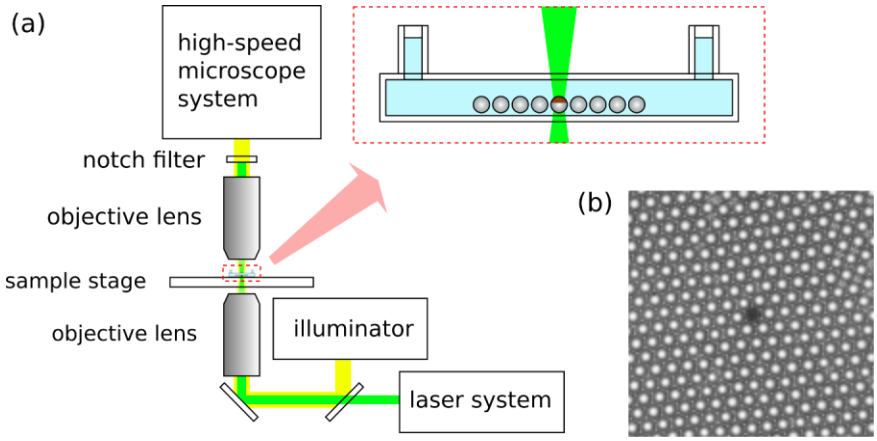

Figure 2.12: Experiment configuration for colloidal systems. (a) SiO_2 particles are injected into micro-fluid cells made of transparent material, in which self-assembled hexagonal lattices are created. The laser beam is merged with the illumination and focused at the same focal plane of the high-speed imaging system. The laser is targeted at the coated SiO_2 particles at the center of the lattice. The resultant response is measured by the high-speed imaging system above the sample. (b) Hexagonal lattice of SiO_2 micro-colloids.

2.5. Software system and lattice construction

To take full advantage of the ability of the experimental system, we used LabVIEW to create a united software interface to communicate with all of the instruments built within the apparatus. Each instrument is controlled by individual LabVIEW blocks that reproduce the physical user interfaces. These blocks are written following the programming architecture of queued state machines. To increase the flexibility of operation, each device can be detached or installed independently in experiments. When hardware failures (such as a loose cable) are detected, the control program automatically disables the corresponding LabVIEW block(s) to prevent damage to the instruments.

A central controlling block communicates with all blocks, as well as with pre-written queue commands in each LabVIEW block. The device blocks communicate with each other through the central controlling block. All steps of the experiments are decomposed into lists of sequential commands. The controlling block ensures that each step of an experiment is being successfully performed in the correct order. This automated control system minimizes experimental errors.

On top of the software system, we developed a sophisticated particle assembling and positioning subroutine that controls the micro-manipulator in order to create the desired configuration of micro-particles on the micro-structure support. Before the process begins, the location of all particles is detected by processing all images of the microscope sequence. The program then automatically generates a sequence of micro-manipulator operations, which is then sent to the LabVIEW controlling blocks. An example of particle assembly and positioning is given in Fig. 2.13, in which the goal is to relocate the two particles to the targeted position marked by the red crosses. The micro-manipulator moves micro-particles by physically pushing them from one side. Figure 2.13a-d shows four basic manipulations of micro-particles along a v-groove, including pushing the particles to the left (or right) and separating particles that are in contact. The positioning of the particles is completed using the following steps: (i-iii) open a small gap between the two particles in contact by lightly brushing on one of the particles from the top; (iv-v) after enough space is available, separate the two particles; and (vi-viii) push the micro-particles to the target position. The central controlling block monitors the progress and completion of each step. If one of the steps fails, our algorithm re-sends the same step to the micro-manipulator or re-generates the entire procedure, if necessary.

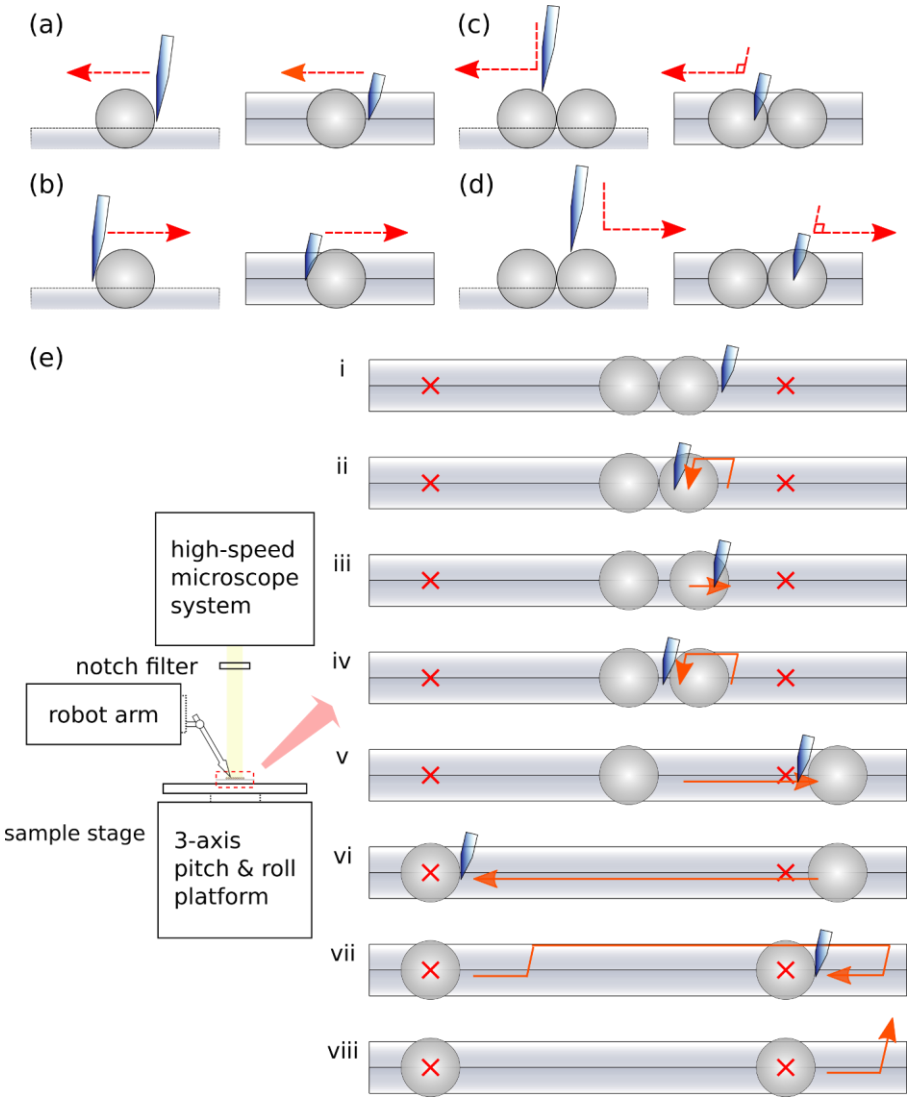

Figure 2.13: An example of the procedure for positioning and assembling micro-particles. (a-d) Schematic of four basic manipulations of a micro-particle, including pushing the particles to the left (right) and gently touching the particle from the top to open up gaps. (e) Procedures of relocating micro-particles to the two targeted positions that are marked by the red crosses. i-iii) open a small gap between the two particles in contact by lightly brushing on one of the particles from the top; iv-v) after enough space is available, separate the two particles; vi-viii) push the micro-particles to the target position.